MOLECULAR AND CELLULAR BIOLOGY, Aug. 2003, p. 5614–5624 Vol. 23, No. 16
0270-7306/03/$08.00+0 DOI: 10.1128/MCB.23.16.5614–5624.2003

Potential Role for ADAM15 in Pathological Neovascularization in Mice

Keisuke Horiuchi,[1] Gisela Weskamp,[1] Lawrence Lum,[1] Hans-Peter Hammes,[2] Hui Cai,[1,3] Thomas A. Brodie,[4] Thomas Ludwig,[5] Riccardo Chiusaroli,[6] Roland Baron,[6] Klaus T. Preissner,[7] Katia Manova,[8] and Carl P. Blobel[1]*

Cellular Biochemistry and Biophysics Program[1] and Molecular Cytology Core Facility, Sloan-Kettering Institute,[8] Memorial Sloan-Kettering Cancer Center, and Cell Biology and Molecular Biology Program, Weill Graduate School of Medical Science of Cornell University,[3] New York, New York 10021; Department of Medicine, University of Heidelberg, 68167 Mannheim,[2] and Department of Biochemistry, Justus-Liebig University, D-35385 Giessen,[7] Germany; Department of Pathology, GlaxoSmithKline, Research Triangle Park, North Carolina 27709[6]; Department of Anatomy and Cell Biology and Institute of Cancer Genetics, Columbia University, New York, New York 10032[5]; and Department of Orthopaedics and Cell Biology, Yale University School of Medicine, New Haven, Connecticut 06510[6]

Received 13 March 2003/Returned for modification 22 April 2003/Accepted 19 May 2003

ADAM15 (named for a disintegrin and metalloprotease 15, metargidin) is a membrane-anchored glycoprotein that has been implicated in cell-cell or cell-matrix interactions and in the proteolysis of molecules on the cell surface or extracellular matrix. To characterize the potential roles of ADAM15 during development and in adult mice, we analyzed its expression pattern by mRNA in situ hybridization and generated mice carrying a targeted deletion of ADAM15 (*adam15*$^{-/-}$ mice). A high level of expression of ADAM15 was found in vascular cells, the endocardium, hypertrophic cells in developing bone, and specific areas of the hippocampus and cerebellum. However, despite the pronounced expression of ADAM15 in these tissues, no major developmental defects or pathological phenotypes were evident in *adam15*$^{-/-}$ mice. The elevated levels of ADAM15 in endothelial cells prompted an evaluation of its role in neovascularization. In a mouse model for retinopathy of prematurity, *adam15*$^{-/-}$ mice had a major reduction in neovascularization compared to wild-type controls. Furthermore, the size of tumors resulting from implanted B16F0 mouse melanoma cells was significantly smaller in *adam15*$^{-/-}$ mice than in wild-type controls. Since ADAM15 does not appear to be required for developmental angiogenesis or for adult homeostasis, it may represent a novel target for the design of inhibitors of pathological neovascularization.

Metalloprotease-disintegrins (ADAMs) are a family of membrane-anchored glycoproteins that are related to snake venom metalloproteases and integrin ligands, termed disintegrins. ADAMs have been implicated in fertilization, myogenesis, neurogenesis, and protein ectodomain shedding (for recent reviews, see references 5, 55, 62, and 63). ADAMs are also thought to have roles in cell-cell adhesion, for example, through interactions with integrins (9, 18, 49) or syndecans (32, 71). Over 30 ADAMs have been identified to date, and yet the function of less than a third of these proteins during development and in adulthood has been characterized. ADAM1 and -2 (fertilin α and β) and ADAM3 have critical roles in fertilization (12, 13, 50, 64). ADAM9 and -12 are not required for development or adult survival (39, 76), although ADAM12 reportedly has a role in processing the heparin-binding epidermal growth factor (EGF)-like growth factor HB-EGF (3), in adipogenesis and myogenesis (34, 39), and in the pathology of muscular dystrophy (38). ADAM13 has been implicated in cranial neural crest migration in *Xenopus laevis* (2). The tumor necrosis factor alpha-converting enzyme (TACE/ADAM17) has a role in releasing the ectodomain of a number of physiologically relevant proteins, including tumor necrosis factor alpha (4, 47); ligands of the EGF receptor, such as HB-EGF (45, 70) and transforming growth factor α (52); and the amyloid precursor protein (8). ADAM17/TACE is essential for survival of newborn mice, presumably because transforming growth factor α and other ligands of the EGF receptor require functional TACE for their proper activation (52). ADAM10/KUZ has a critical role in Notch signaling and is required for early development in *Drosophila melanogaster* and mice (19, 24, 59, 68). In *Caenorhabditis elegans*, the related SUP-17 is also a key component of the Notch signaling pathway (75). Finally, mice carrying a genetrap insertion in ADAM23 uncovered an essential role for this gene in mouse brain development (46).

The goal of the present study was to investigate the role of the widely expressed ADAM15 in mouse development and in adult mice. Human ADAM15 was first discovered in a screen for novel ADAMs by PCR (28, 37) and was named metargidin because it carries an RGD sequence in a position similar to that in snake venom disintegrins (37). However, the mouse and rat orthologues of ADAM15 lack an RGD sequence (7, 42), arguing against a conserved role of ADAM15 as ligands for RGD-binding integrins in these two rodents. Although human ADAM15 can indeed interact with RGD-binding integrins (αvβ3 and α5β1) (48, 80), mouse ADAM15 does not (18). Instead, mouse ADAM15 has been implicated as a ligand for

* Corresponding author. Mailing address: Cellular Biochemistry and Biophysics Program, Sloan-Kettering Institute, Memorial Sloan-Kettering Cancer Center, Box 368, 1275 York Ave., New York, NY 10021. Phone: (212) 639-2915. Fax: (212) 717-3047. E-mail: c-blobel@ski.mskcc.org.

integrin α9β1 (17, 18). Both mouse and human ADAM15 contain a catalytic site consensus sequence for zinc-dependent metalloproteases, and purified recombinant ADAM15 is catalytically active (44). The cytoplasmic domain of ADAM15 contains potential signaling motifs, such as SH3 ligand domains, and has been shown to interact with Src family members (54), as well as with two molecules that have a role in intracellular protein transport: endophilin and sortin nexin9 (30).

In the present study we evaluated the expression of ADAM15 in mouse development and in adult animals, and we analyzed the effect of inactivating ADAM15 by a targeted deletion in mice. Although ADAM15 is ubiquitously expressed, prominent expression was found in the vasculature, bone, and brain. Mice carrying a null mutation in ADAM15 are viable and fertile without any evident pathological phenotypes. However, compared to the wild-type controls, *adam15*$^{-/-}$ mice show a strongly reduced angiogenic response in a model of hypoxia-induced proliferative retinopathy, and significantly smaller tumors develop after implantation of melanoma cells. These results suggest that ADAM15 has an important role in mediating pathological neovascularization.

MATERIALS AND METHODS

Materials. Restriction enzymes and molecular biology reagents were purchased from Roche Diagnostics (Mannheim, Germany) and New England Biolabs (Beverly, Mass.), and chemicals were from Sigma (St. Louis, Mo.), except where a different supplier is indicated.

Construct design. A cDNA fragment comprising bp 85 to 1103 of mouse ADAM15 cDNA (GenBank accession no. NM_009614) was used to screen a 129/ SVJ genomic library (Stratagene, La Jolla, Calif.). A putative ADAM15 genomic clone was characterized by restriction mapping and was sequenced with gene-specific primers. The most 5′ exon containing the initial methionine residue and the first 27 amino acids of the ADAM15 protein were deleted by insertion of the MCI-neo selectable marker. The resulting cassette containing both 5′ and 3′ homology regions (5.4 kb) was then placed into a β-actin-driven diphtheria toxin vector (78) for negative selection.

Generation of targeted ES cells. Primary mouse fibroblasts were isolated, mitotically inactivated, and used as feeders (58) for 129/SVJ embryonic stem (ES) cells that had been electroporated with 30 μg of linearized targeting vector. The stem cells were kept in selection medium (350 μg of G418/ml) for 7 to 10 days before colonies were picked, expanded, and screened by Southern blot analysis (76). Correct integration of the targeting construct was confirmed with 5′ and 3′ specific probes and a *neo* probe. The targeting efficiency was ca. 10%.

Generation of mice lacking ADAM15. ES cells carrying a properly targeted ADAM15 allele were injected into blastocysts from C57BL/6J mice in order to generate chimeric offspring. The resulting chimeric male mice with a high percentage of the agouti coat color (indicating a high degree of chimerism) were mated with C57BL/6J or 129/SvJ females. Offspring from matings with C57BL/6J mice were of mixed genetic background, whereas offspring from matings with the 129/SvJ background produced inbred animals of the 129/SvJ background. Finally, mixed-background 129/SvJ/C57BL/6J *adam15*$^{+/-}$ mice were backcrossed six times with inbred C57BL/6J mice to generate *adam15*$^{-/-}$ mice with a predominantly C57BL/6J background.

Production of monoclonal and polyclonal antibody to ADAM15. An ADAM15 ectodomain fusion protein with the immunoglobulin G (IgG) Fc domain (ADAM15-EC-Fc) was used to immunize *adam15*$^{-/-}$ mice by intraperitoneal injection with ca. 25 μg of purified recombinant protein emulsified 1:1 in Titermax at 3-week intervals. Once a good immune response was confirmed by Western blot and enzyme-linked immunosorbent assay analysis on purified ADAM15-EC-Fc protein, monoclonal antibodies were produced according to standard procedures (76). Hybridomas producing monoclonal antibodies to ADAM15 were cloned three times by limiting dilution, adapted to serum-free conditions, and produced in a MiniPerm bioreactor system (Sartorious, Edgewood, N.Y.). Furthermore, a polyclonal rabbit antiserum against ADAM15 was produced by injecting 25 μg of ADAM15-EC-Fc into female New Zealand White rabbits at intervals of 4 weeks (Covance, Princeton, N.J.).

Western blot analysis. Western blot analysis of ADAM15 protein in mouse tissues and cell lines was performed as previously described (76, 77).

In situ hybridization. Timed matings were set up to generate embryos at different stages of gestation (i.e., embryonic day 7.5 [E7.5], E9.5, E11.5, E13.5, and E15.5) for an analysis of ADAM15 expression by mRNA in situ hybridization. Mouse embryos were fixed in 4% paraformaldehyde overnight at 4°C. In order to prepare adult mouse brains for in situ hybridization, mice were first anesthetized and then transcardially perfused with phosphate-buffered saline (PBS), followed by perfusion with 4% paraformaldehyde. The brains were then removed and postfixed in 4% paraformaldehyde overnight at 4°C. Graded series of ethanol were then used to dehydrate the fixed embryos and brains. The dehydrated tissues were cleared with Histoclear, embedded in paraffin, cut into 8-μm paraffin sections, and mounted on Fisher Superfrost-Plus slides. Single-stranded ^{33}P-labeled ADAM15 RNA probes were prepared from linearized plasmids with T7 or Sp6 RNA polymerases, and ribonucleotide triphosphate mix containing 12 μM cold UTP and 4 μM hot UTP. The antisense probe hybridized with a 455-bp ADAM15 cDNA C-terminal fragment from the *Hind*III to *Xho*I site. The corresponding sense RNA strand served as a negative control. These probes were also used in Northern blot analysis of the RNAs isolated from mouse embryos to confirm their specificity. The RNA in situ hybridization procedure was essentially as described previously (43, 76).

Histopathology and clinical pathology. One-year-old wild-type or *adam15*$^{-/-}$ mice (five males and five females) of mixed genetic background were sacrificed for necropsy and histopathological analysis. Liver, spleen, kidney, brain, and heart were harvested, weighed, and fixed in 10% buffered formalin. Bouin's fixative was used to preserve eyes and testes. Terminal blood samples were prepared for clinical chemistry analysis (with a Roche Diagnostics Hitachi Analyser model 911/917), and the total protein, albumin, alkaline phosphatase, glutamic pyruvic transaminase, glutamic oxaloacetic transaminase, total bilirubin, blood urea nitrogen, cholesterol, glucose, Na^+, K^+, and Cl^- contents were measured. The following tissues were stained with hematoxylin and eosin after fixation and examined microscopically: adrenals, aorta, brain, cecum, colon, duodenum, epididymides, eyes (including the optic nerve), gallbladder, Harderian gland, heart, ileum, jejunum, kidneys, liver, lungs, lymph nodes (mandibular and mesenteric), esophagus, ovaries, pancreas, peripheral nerve, pituitary, prostate, rectum, salivary glands, seminal vesicles, skeletal muscle, skin (and mammary glands), spinal cord (cervical, thoracic, and lumbar portions), spleen, sternum (and bone marrow), stomach, testes, thymus, thyroids (and parathyroids), tongue, trachea, urinary bladder, uterus, and vagina. Brains were also stained with Congo red and Bielschowsky's silver stain. Furthermore, five each 19-month-old male and female *adam15*$^{-/-}$ and wild-type mice of mixed genetic background, as well as five each 14- to 18-month-old male and female *adam15*$^{-/-}$ and wild-type mouse of the 129/SvJ background, were subjected to a limited analysis of liver, heart, gallbladder, mammary gland, and uterus because of minor pathological findings in these tissues in some of the 1-year-old *adam15*$^{-/-}$ mice.

Flow cytometric analysis. Axillary and brachial peripheral lymph nodes were isolated from four age-matched wild-type and *adam15*$^{-/-}$ mice in order to generate single cell suspensions. These were stained with fluorescein isothiocyanate-conjugated anti-T-cell receptor (clone H57-597) and phycoerythrin-conjugated anti-CD24 (clone M1/69) and then analyzed with an LSR analytical cytometer (BD Immunocytometry Systems, San Jose, Calif.). The fluorescently labeled antibodies were produced, purified, and conjugated at the Memorial Sloan-Kettering Cancer Center (MSKCC) Monoclonal Antibody Core Facility.

Immunohistochemistry. Embryos and adult tissues were fixed in 4% paraformaldehyde overnight at 4°C. The fixed specimens were washed two times with PBS, immersed in 30% sucrose overnight at 4°C, and then frozen in Tissue-Tek O.C.T. compound (Sakura Finetek, Torrance, Calif.). Sections (10 or 14 μm) were cut and mounted on Fisher SuperFrost slides. The sections were postfixed with ice-cold acetone for 10 min, immersed in 0.1% H_2O_2 to inactivate the endogenous peroxidase, preincubated with 10% normal goat serum–2% bovine serum albumin–PBS for 30 min, and then incubated for 3 h with anti ADAM15-EC-Fc antiserum (see above) or platelet endothelial cell adhesion molecule-1 (PECAM-1/CD31) antibody (Santa Cruz Biotech, Santa Cruz, Calif.). Bound antibody was detected with biotinylated conjugated goat anti-rabbit IgG antibody and by standard Avidin-Biotin complex method according to the manufacturer's instructions (Vector Laboratories, Burlingame, Calif.). After development of the color reaction with diaminobenzidine solution (Vector Laboratories), sections were counterstained with hematoxylin.

Mouse ROP model. The response of wild-type and *adam15*$^{-/-}$ mice to relative hypoxia was assessed by using the retinopathy of prematurity (ROP) model essentially as described previously (23, 67). Briefly, the animals were placed in a Plexiglas chamber and exposed to an oxygen concentration of 75% from post-

natal day 7 to 12 (a chamber and oxygen regulator, Proox model 110, were supplied by Reming Bioinstruments, Redfield, N.Y.), along with their nursing mother. At postnatal day 12 (P12), the animals were returned to normal room air. The resulting relative hypoxia triggers a proliferative response in the retinal vasculature. At 5 days after the return to normoxic conditions (i.e., P17), the animals were sacrificed. Their eyes were removed, fixed in 4% paraformaldehyde, embedded in paraffin, sectioned (6-μm thickness), and stained with hematoxylin and eosin. Histological evaluation of vascularization was performed by counting endothelial nuclei on the vitreal side of the internal limiting membrane as previously described (67). About 150 sections were prepared from each eye, and two to five sections on each side of the optic nerve, 30 to 90 μm apart, were used for the evaluation in a double-blind manner. The number of endothelial nuclei for each eye was averaged, and the unpaired Student *t* test (equal variation, two sided) was used to statistically evaluate the difference between *adam15*$^{-/-}$ and wild-type mice.

Cell culture. Human umbilical vein endothelial cells (HUVECs) were purchased form VEC technologies (Rensselaer, N.Y.) and grown in EGM medium (BioWhittaker, Walkersville, Md.) as instructed by the manufacturer. Recombinant human vascular endothelial growth factor (VEGF) and basic fibroblast growth factor (bFGF) were purchased from R&D Systems (Minneapolis, Minn.). HUVECs were grown to confluence and, prior to stimulation with either VEGF or bFGF, cells were serum-starved in M-199 medium containing 1% fetal calf serum for 12 h. The cells were then incubated in M-199 medium containing 1% fetal calf serum with or without either VEGF (20 ng/ml) or bFGF (20 ng/ml) for 3 and 9 h. Cell lysates were collected and analyzed by Western blot as described previously (76).

Heterotopic injection of B16F0 mouse melanoma cells. Age- and sex-matched wild-type and *adam15*$^{-/-}$ mice of either a mixed genetic background (129/SvJ and C57BL/6J) or an inbred background (C57BL/6J) were given single subcutaneous injections of 10^6 B16F0 mouse melanoma cells resuspended in PBS. The animals were sacrificed 2 to 3 weeks after injection, depending on the severity of the tumor burden, and the tumors were removed and weighed. For quantitation and comparison of individual trials, the average weight of tumors from wild-type controls in a given trial was used as a reference to calculate the weight of each tumor as a percentage of the wild-type average. The unpaired Student *t* test was used for statistical evaluation as described above. Immunofluorescence was further performed to evaluate the vascularity of the tumor specimens. The frozen sections were prepared as described above and incubated with anti-PECAM antibody (BD Biosciences/Pharmingen, San Diego, Calif.). Bound antibodies were detected by Cy3-conjugated AffiniPure donkey anti-rat IgG (Jackson ImmunoResearch, West Grove, Pa.). Quantitative analysis was performed by using Scion Image (beta 4.0.2).

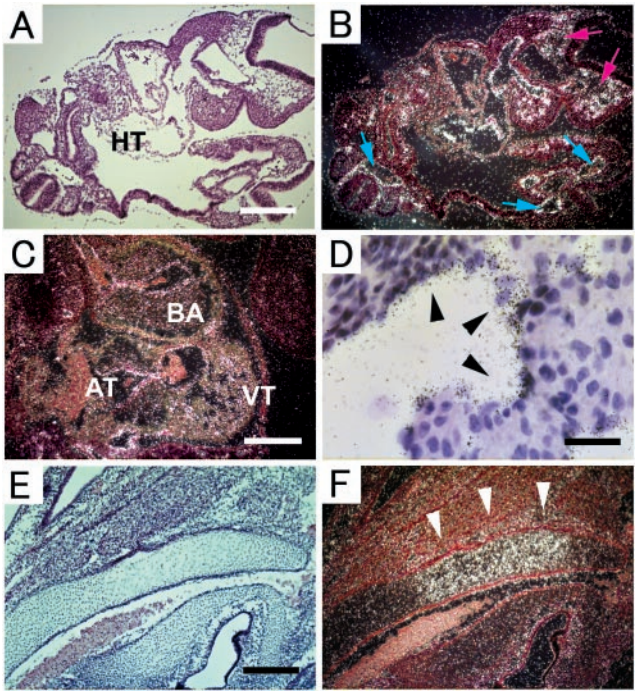

FIG. 1. Expression of ADAM15 mRNA in mouse embryos. All sections were hybridized with an antisense ADAM15 probe (as described in Materials and Methods). Digital images were obtained by bright-field (A, D, and E) and dark-field (B, C, and F) microscopy. (A and B) Section of E9.5 embryo, showing a prominent expression in mesenchymal tissue in the developing head (red arrows), developing heart (HT), arteries (blue arrows). Scale bar, 100 μm. (C) Section of the heart of an E11.5 embryo. Strong expression was observed in the surface lining the ventricle (VT), atrium (AT), and bulbus arteriosus (BA). Scale bar, 200 μm. (D) Bright-field view (magnification, ×400) of the ventricle of an E13.5 embryo shows high-level expression in the endocardium (arrowheads). Scale bar, 50 μm. (E and F) In the cartilage primordium of occipital bone of an E16.5 embryo, positive signals can be seen in hypertrophic cells (arrowheads). Scale bar, 200 μm.

RESULTS

Analysis of ADAM15 expression during development and in adult mice. The mRNA expression pattern of ADAM15 was evaluated by mRNA in situ hybridization in developing and adult mice. This revealed a quite ubiquitous expression pattern of ADAM15 mRNA, as well as enhanced expression in certain cells and tissues. At E9.5 and thereafter, prominent expression of ADAM15 was found in the vasculature, including the ventral and dorsal aorta and the caudal artery (Fig. 1A to D). In the developing heart, positive signals were observed in the endocardium and the blood vessels of the ventricle, bulbus arteriosus, and atrium (Fig. 1C and D). Furthermore, ADAM15 was highly expressed in a subpopulation of cells in the bone during development that resemble hypertrophic chondrocytes (Fig. 1E and F).

The pronounced expression of ADAM15 mRNA in the vasculature and endocardium (Fig. 1B to D) prompted further evaluation of ADAM15 protein expression by immunohistochemistry. This confirmed that ADAM15 is strongly expressed in large vessels and in the endocardium at E13.5 (Fig. 2A) and also revealed strong expression in capillaries (Fig. 2C and E). When adjacent sections were stained with an anti-PECAM-1 antibody, a marker for endothelial and endocardial cells, an almost identical staining pattern was observed (Fig. 2B, D, and F). The expression of ADAM15 in endothelial cells was confirmed by probing a Western blot of HUVEC extract with antibodies to human ADAM15 (Fig. 2G).

An evaluation of ADAM15 expression in adult tissues showed prominent expression in specific brain areas, including the hippocampus, cerebellum, pons, thalamus, cortex, and olfactory bulb (Fig. 3A to F and data not shown). In the hippocampus, ADAM15 is expressed in the pyramidal layer of the hippocampus proper and the granular layer of the dentate gyrus (Fig. 3A and B). In the cerebellum, ADAM15 is predominantly expressed in the Purkinje cell layer (Fig. 3C and D). In the pons, ADAM15 was expressed mostly in pontine nuclei (Fig. 3E and F). The expression pattern of ADAM15 in mouse brain thus closely resembles the expression that has been described for rat brains (7).

Targeted deletion of ADAM15 in mice. In order to learn more about the function of ADAM15 in mice, a targeted deletion of the exon carrying the initial methionine of ADAM15 was performed (Fig. 4A and B; see Materials and Methods for details). When heterozygous mice of mixed genetic background (129/SvJ and C57BL/6J) or of inbred genetic back-

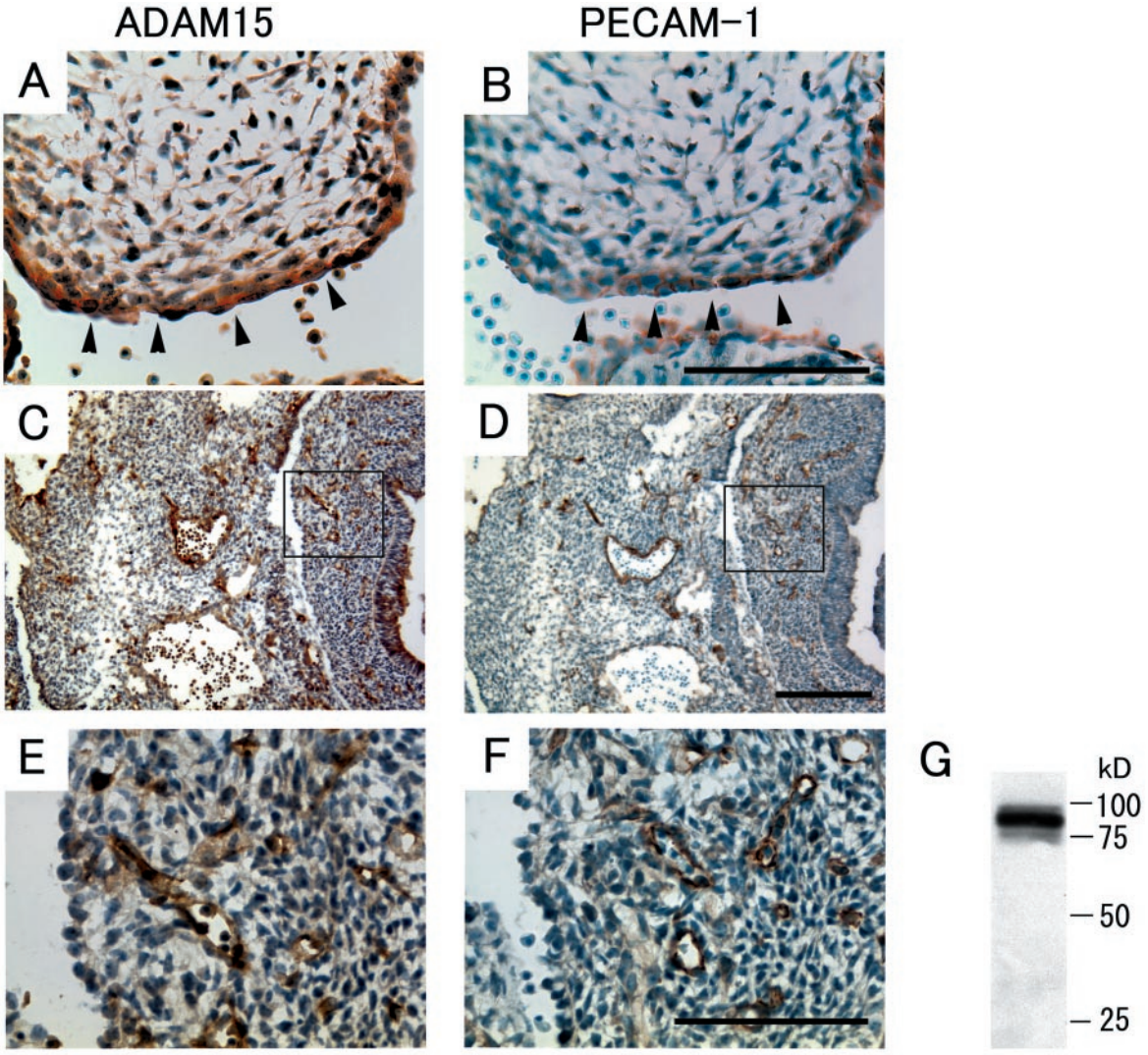

FIG. 2. Expression of ADAM15 (A, C, and E) and PECAM-1 (B, D, and F) in the endocardium and in the developing vasculature at E13.5. (A and B) Consecutive serial sections of the endocardial cushion of the heart of an E13.5 embryo stained with anti-ADAM15 antibody (A) or anti-PECAM-1 antibody (B). Strong expression of ADAM15 can be seen in endocardial cells, which here line the surface of the endocardial cushion. These cells are also positive for PECAM-1 staining. Scale bar, 100 μm. (C to F) Consecutive sections of the lower trunk and abdomen of an E13.5 embryo reveal an almost identical staining pattern for ADAM15 (C) as for PECAM-1 (D). Scale bar, 200 μm. At high magnification (the boxed areas in panels C and D), positive-staining reveals similar capillary structures in the sections stained with ADAM15 (E) and PECAM-1 (F). Scale bar, 100 μm. The staining of endothelial cells is specific for ADAM15, since it was not observed in mice lacking ADAM15 (see below, Fig. 4). However, the staining of blood cells by the ADAM15 antibody is nonspecific, since this staining is not abolished in *adam15*$^{-/-}$ mice (see Fig. 4D). (G) Western blot analysis confirmed that ADAM15 is expressed in HUVECs.

ground (129/SvJ or C57BL/6J) were mated, the genotype of the offspring followed a Mendelian distribution pattern, regardless of the background (Table 1). Western blot analysis of mouse heart extracts confirmed that the expression of the ADAM15 protein was abrogated in *adam15*$^{-/-}$ mice (Fig. 4C). The sections of *adam15*$^{-/-}$ mice immunostained with anti-ADAM15 antibody revealed no positive staining in the vessels, thus corroborating the specificity of the antibody (Fig. 4D).

Mice lacking ADAM15 were frequently compared to age- and gender-matched wild-type littermates with respect to their appearance, behavior when handled, weight gain after birth, and average weight of adults up to 2 years of age (data not shown). In all respects, *adam15*$^{-/-}$ mice were indistinguishable from control littermates, regardless of the genetic background. Matings of *adam15*$^{-/-}$ mice resulted in viable and healthy litters, with normal litter sizes for each of the genetic backgrounds tested. Furthermore, when 35 male and 35 female *adam15*$^{-/-}$ and wild-type mice of each genetic background were observed for 2 years, no significant difference in mortality or morbidity was seen.

Histological analysis of heart, bone, brain, and kidney morphology in *adam15*$^{-/-}$ mice. Because ADAM15 is strongly expressed in the endocardium and in developing bone, we examined sections of *adam15*$^{-/-}$ embryos and wild-type littermates at different embryonic stages in order to compare the morphology of these structures, as well as of other tissues. When

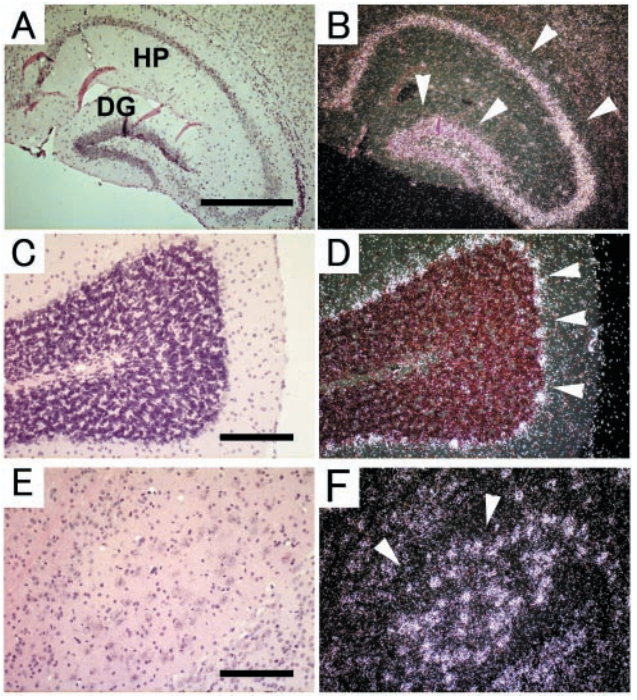

FIG. 3. Expression of ADAM15 mRNA in adult mouse brain. Brain sections were hybridized with antisense ADAM15 mRNA probe and analyzed by using bright-field (A, C, and E) and corresponding dark-field (B, D, and F) images. Coronal sections through the hippocampus (A and B) show strong expression in the pyramidal layer and in the granular layer (arrowheads). HP, hippocampus proper; DG, dentate gyrus. Strong expression can be seen in the Purkinje cell layer (C and D, arrowheads) and in a subset of cells in the central part of the hypothalamus (E and F, arrowheads). Scale bars: A, 500 μm; C and E, 200 μm.

hearts of E13.5 embryos were stained with PECAM-1 to mark endocardial cells, no difference in the staining pattern was observed between *adam15*$^{-/-}$ and wild-type embryos (Fig. 5A to D). As described above, expression of ADAM15 was found in the developing bone. However, safranin-o and fast green-stained femurs of 4-week-old *adam15*$^{-/-}$ or wild-type mice (Fig. 5E and F) could not be distinguished from each other. Likewise, in a histopathological analysis, sections of adult brains from *adam15*$^{-/-}$ mice stained with cresyl fast violet were indistinguishable from age-matched wild-type brains (Fig. 5G to J and data not shown). Finally, since ADAM15 was recently implicated in migration of glomerular mesangial cells in certain kidney diseases (44), we compared kidneys from wild-type and *adam15*$^{-/-}$ mice. However, we did not find any evident histopathological defect of the kidney or glomeruli in the absence of ADAM15 at the level of light microscopy (Fig. 5K and L). Moreover, there were no abnormalities in a clinical chemistry analysis of serum from *adam15*$^{-/-}$ mice, arguing against a major defect in kidney function. A histopathological analysis of other tissues in age-matched adult *adam15*$^{-/-}$ and wild-type mice also did not uncover morphological aberrations (see Materials and Methods for a listing of the tissues and organs analyzed). Finally, we found no abnormalities in a differential blood count or in the ratio of $CD4^+$ to $CD8^+$ cells in lymph nodes and thymus in *adam15*$^{-/-}$ mice compared to wild-type mice (data not shown). Taken together, no evident histopathological defects were found in the hearts, bones, or other tissues in developing or adult *adam15*$^{-/-}$ mice.

Reduced neovascularization in a mouse model of proliferative retinopathy. The high level of expression of ADAM15 in vascular cells led us to investigate a potential role in pathological neovascularization. For this purpose, we subjected wild-type and *adam15*$^{-/-}$ mice to the ROP model (11, 23, 67). In this model, 7-day-old mice are placed in high oxygen (75%) and are then returned to room air. The resulting drop in oxygen concentration triggers a strong angiogenic stimulus, resulting in pathological neovascularization in the retina (see Materials and Methods for details). In the ROP model, *adam15*$^{-/-}$ mice had a 64% lower angiogenic response on average compared to wild-type controls (wild type, $n = 34$, mean = 44.1 ± 20.0; *adam15*$^{-/-}$, $n = 33$, mean = 15.6 ± 16.2; $P < 0.001$) (Fig. 6A). Western blot analysis demonstrated that ADAM15 protein levels in the retina were upregulated after the relative hypoxic stimulus, whereas no change in ADAM15 protein levels was seen in untreated age-matched controls (Fig. 6B). The increased expression of ADAM15 persisted for 4 days and returned to normal levels within 6 days. Immunohistochemical analysis confirmed the expression of ADAM15 in retinal capillaries, with particularly enhanced expression in new blood vessels that had grown toward or traversed the internal limiting membrane (Fig. 6C). In serial sections, these vessels also stained positively for the endothelial cell marker PECAM-1 (Fig. 6C). To study the possible involvements of VEGF and bFGF in the regulation of ADAM15 protein expression in endothelial cells, HUVECs were incubated with VEGF or bFGF for 3 and 9 h. However, neither of these growth factors significantly affected ADAM15 protein levels compared to untreated control HUVECs (see Fig. 6D).

Reduced growth of B16F0 mouse melanoma cells in *adam15*$^{-/-}$ mice. Tumors must recruit host vessels for survival (10); hence, tumor angiogenesis is a critical factor for tumor growth. To evaluate whether *adam15*$^{-/-}$ mice exhibit a decreased response in a second experimental model for neovascularization, we implanted B16F0 melanoma cells in the flanks of *adam15*$^{-/-}$ mice and wild-type controls. In a mixed background (129/SvJ and C57BL/6), *adam15*$^{-/-}$ mice showed a significant decrease in tumor burden compared to the wild-type controls (Fig. 7A, wild type, $n = 27$, mean = 100 ± 72.3; *adam15*$^{-/-}$, $n = 28$, mean = 34.5 ± 42.0; $P = 0.00013$; see Materials and Methods for details). Similar results were obtained by using *adam15*$^{-/-}$ mice in a C57BL/6 background (Fig. 7B, wild type, $n = 23$, mean = 100 ± 39.8; *adam15*$^{-/-}$, $n = 19$, mean = 67.5 ± 44.5; $P = 0.017$). Despite the significant differences in tumor burden between wild-type and *adam15*$^{-/-}$ mice, the morphological appearance of tumors, as well as the density of PECAM-1-stained blood vessels in nonnecrotic areas of the tumors, were similar in both genotypes (Fig. 7C, wild type, mean = 20.6 ± 5.1 vessels/mm^2; *adam15*$^{-/-}$, mean = 21.3 ± 5.7 vessels/mm^2).

DISCUSSION

The main goal of the present study was to provide insights into the functions of the metalloprotease-disintegrin ADAM15 (metargidin) during development and in adult homeostasis.

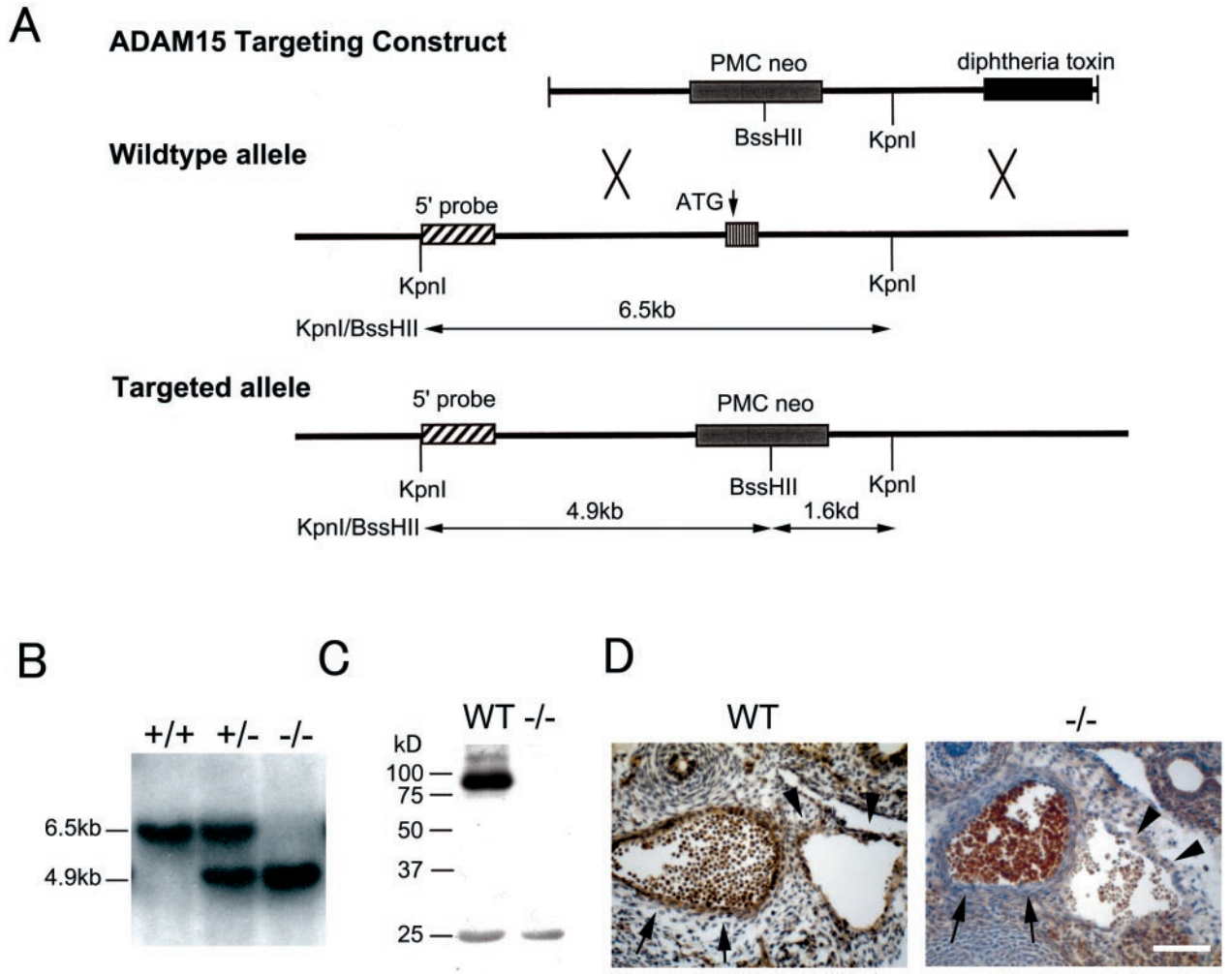

FIG. 4. Targeted mutation of ADAM15. (A) The targeting vector is shown at the top. The targeted exon was disrupted by insertion of a pMC1neoPolyA cassette, which introduces a *Bss*HII site that is not present in the wild-type allele. A diphtheria toxin gene cassette was added at the 3′ end of the targeting construct to select against nonhomologous recombination events. A schematic of the wild-type *adam15* allele is shown in the middle. The position of the 5′ probe used for Southern blot analysis is indicated, as well as the exon that codes for the initial methionine of ADAM15, and *Kpn*I sites. The bottom panel shows key features of the targeted allele. The *Bss*HII site introduced into the targeted allele reduces the length of the *Kpn*I/*Bss*HII genomic fragment recognized by the 5′ probe from 6.5 to 4.9 kb. (B) Southern blot analysis of *Kpn*I/*Bss*HII-digested genomic DNA from wild-type, heterozygous *adam15*$^{+/-}$, and homozygous *adam15*$^{-/-}$ mice. (C) Western blot analysis of heart extracts from wild-type and *adam15*$^{-/-}$ mice confirmed that ADAM15 protein expression is abolished in *adam15*$^{-/-}$ mice. (D) Sections of the descending aorta (arrows) and subcardinal vein (arrowheads) of wild-type (WT) and *adam15*$^{-/-}$ (−/−) E13.5 embryos. An immunohistochemical analysis shows staining of vascular cells in wild-type mice but not in *adam15*$^{-/-}$ mice. Scale bar, 100 μm. This finding confirms that the vascular staining pattern of anti-ADAM15 polyclonal antibodies is specific. In contrast, blood cells within the vessels are stained in both wild-type and *adam15*$^{-/-}$ mice, and therefore this staining is not specific for ADAM15. The polyclonal anti-ADAM15 antibodies used in panels C and D and in Fig. 2 were from the same bleed of a New Zealand White rabbit that was immunized with an Fc fusion protein with the ectodomain of mouse ADAM15.

Our results demonstrate that ADAM15 expression can be detected in most tissues in developing and adult mice (42), with the highest levels of expression in vascular cells, the endocardium, hypertrophic cells in developing bone, and specific regions of the brain. However, the morphology of these and other tissues was not noticeably altered in developing or adult *adam15*$^{-/-}$ mice compared to age-matched wild-type controls. Furthermore, *adam15*$^{-/-}$ mice appeared healthy, were fertile, and did not display any evident pathological phenotypes. The lack of clear developmental or pathological phenotypes in *adam15*$^{-/-}$ mice may be due to functional redundancy with, or compensation by other ADAMs or other molecules. ADAM15

TABLE 1. Results of *adam15*$^{+/-}$ × *adam15*$^{+/-}$ matings in 129/SvJ and C57BI/6J genetic backgrounds

Mouse strain	No. (%) of offspring		
	adam15$^{+/+}$	*adam15*$^{+/-}$	*adam15*$^{-/-}$
129/SvJ	45 (23.9)	99 (52.7)	44 (23.4)
C57BI/6J	49 (29.5)	83 (50.0)	34 (20.5)
129/SvJ and C57BL/6J[a]	49 (25.9)	89 (47.1)	51 (27.0)

[a] Mixed genetic background.

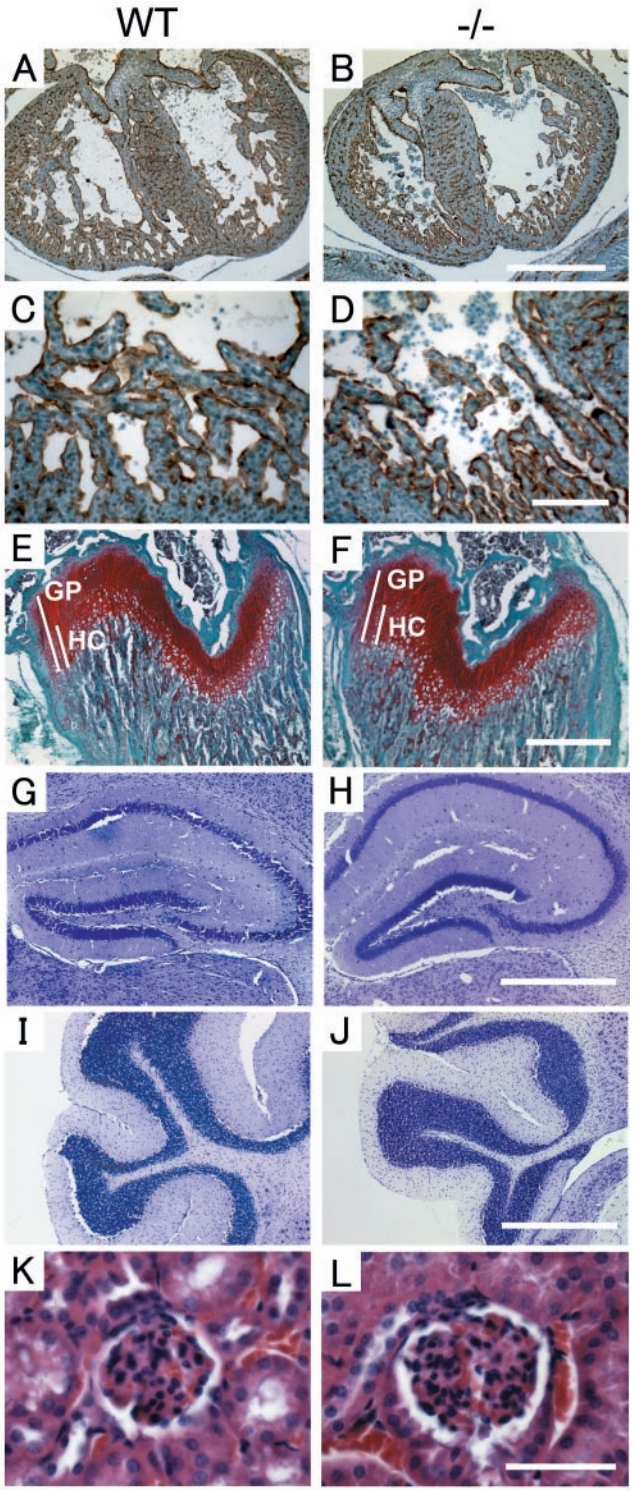

FIG. 5. Histological sections of the heart, bone, brain and renal glomerulus of wild-type (WT) and *adam15*$^{-/-}$ (−/−) mice. (A to D) Sections of the heart are from E13.5 wild-type (A and C) and *adam15*$^{-/-}$ (B and D) embryos stained with PECAM-1, a marker for endothelial and endocardial cells (magnification, ×50; scale bar, 500 μm [A and B]; magnification, ×200; scale bar, 100 μm [C and D]). (E and F) Section of the distal femur of 4-week-old wild-type (E) or *adam15*$^{-/-}$ (F) mice stained with safranin-o (which stains cartilage in red), fast green, and hematoxylin. The overall thickness of the growth plate (GP) and the relative size of the zone of hypertrophic cells (HC) were comparable in wild-type and *adam15*$^{-/-}$ mice. Scale bar, 500 μm. (G to J) Morphological comparison of the hippocampus (G and H) and cerebellum (I and J) of adult wild-type (G and I) and *adam15*$^{-/-}$ (H and J) mice stained with cresyl violet. No histological aberrations were apparent in the brains of *adam15*$^{-/-}$ mice. Scale bar, 500 μm. (K and L) Kidney glomerulus of a wild-type (K) and *adam15*$^{-/-}$ (L) mouse are indistinguishable from each other at the light-microscopic level at a magnification of ×400. Scale bar, 50 μm.

may also have nonessential, but nevertheless critical roles in certain cells and tissues, which might only be elucidated through appropriate functional challenges of *adam15*$^{-/-}$ mice.

Because of the particularly high level of expression of ADAM15 in vascular cells, we decided to investigate a potential role in pathological neovascularization. For this purpose, we decided to evaluate the function of ADAM15 in a model for proliferative retinopathies: the ROP model. In this model, the expression of ADAM15 is upregulated in the retinas of wild-type animals after the relative hypoxic stimulus that serves as a trigger for neovascularization. When *adam15*$^{-/-}$ mice were subjected to the ROP model, the growth of new blood vessels was strongly decreased compared to wild-type controls. Taken together, these results suggest that ADAM15 has a critical role in pathological neovascularization.

To corroborate the findings of the ROP model, *adam15*$^{-/-}$ mice were subjected to a second disease model in which neovascularization has a prominant role, the growth of heterotopically injected tumor cells. In *adam15*$^{-/-}$ mice, tumors that developed from implanted mouse melanoma cells were significantly smaller than in wild-type controls. The decreased tumor burden in *adam15*$^{-/-}$ mice is consistent with a role for ADAM15 in neovascularization. However, no detectable abnormalities in the number or distribution of blood vessels were evident in tumors that developed in *adam15*$^{-/-}$ mice. This raises the possibility that the contribution of ADAM15 to growth of implanted tumors is independent of its putative role in neovascularization. ADAM15 could, for example, release a host-derived growth factor that stimulates tumor growth directly without affecting angiogenesis. Nonetheless, the normal appearance of vessels in heterotopic tumors in *adam15*$^{-/-}$ mice does not rule out the possibility that ADAM15 may have a function in neovascularization in tumors similar to the role it has in the ROP model. Relatively smaller tumors with apparently normal vasculature in *adam*$^{-/-}$ mice could be explained by defects in certain aspects of neovascularization, such as a delay in the initiation of new vascular sprouts or in the growth rate of new vessels. These and other possibilities will be addressed in future studies.

In light of the domain organization of ADAM15, several potential mechanisms underlying a role in pathological neovascularization can be considered. The relevant protein domains are the metalloprotease domain, which is catalytically active in ADAM15 (44); the disintegrin domain and cysteine-rich region, which may mediate cell-cell or cell matrix interaction; and the cytoplasmic domain, which may have a role in signaling or intracellular transport (6, 55, 62, 63).

Several ADAMs have been implicated in the proteolytic release of molecules from the cell surface, a process termed protein ectodomain shedding (3, 4, 14, 21, 39, 41, 47, 51, 56,

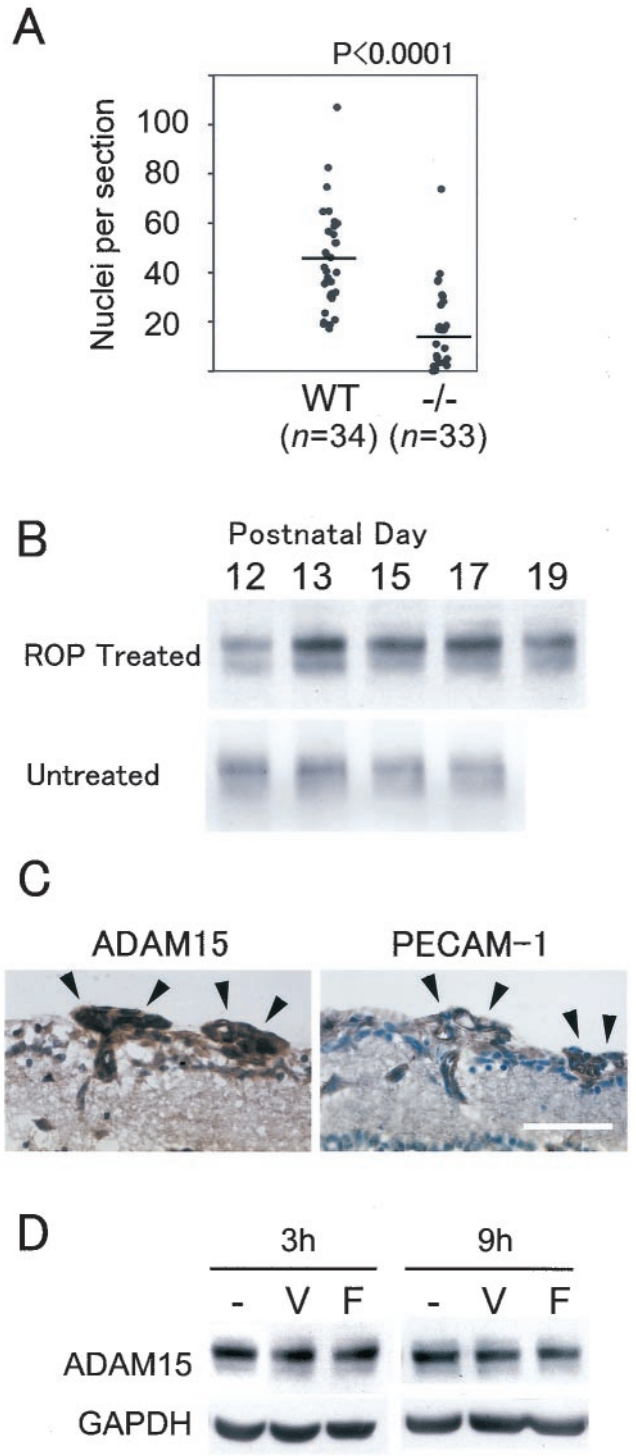

FIG. 6. Decreased retinal angiogenesis in *adam15*$^{-/-}$ mice in a mouse ROP model. (A) Wild-type (WT) and *adam15*$^{-/-}$ (−/−) mice were subjected to the ROP model, and the ensuing neovascularization in the retina was evaluated as described in Materials and Methods. A significantly decreased angiogenic response was observed in *adam15*$^{-/-}$ mice compared to wild-type animals. The bars represent the average value. (B) Western blot analysis of ADAM15 expression in the retinas of mice subjected to the ROP model, analyzed at different time points after the return to room air (top panel). As a control, a Western blot of retinas from age-matched untreated mice is shown in the lower panel. Each lane contains the lysate of one retina. ADAM15 expression is significantly upregulated 1 day after the return to room air (P13). The upregulation persists for at least 4 days and ADAM15 expression in the retina returns to the basal levels by P19. (C) Serial sections of the retinas of wild-type mice subjected to the ROP model stained with ADAM15 or PECAM-1. Prominent expression of ADAM15 is found in the endothelial cells migrating into the vitreous body. The staining pattern of PECAM-1 is very similar to that of ADAM15. Scale bar, 50 μm. (D) Confluent HUVECs were incubated without additional supplement (lanes −), with VEGF (20 ng/ml) (lanes V), or bFGF (20 ng/ml) (lanes F) after 12 h of starvation. Neither addition of VEGF nor addition of bFGF detectably affected the expression level of ADAM15 protein in HUVECs.

65). If the catalytic activity of ADAM15 is important for a function in angiogenesis, ADAM15 may act as a sheddase of one or more cell surface molecules with a role in angiogenesis. In principle, substrates of ADAM15 could include an adhesion protein that must be cleaved to allow endothelial cell sprouting, a membrane-bound angiogenic factor that must be released to become active, a receptor that must be activated by proteolysis, or an inhibitory receptor that must be inactivated. Specific candidate substrates for ADAM15 in the context of neovascularization would then include Notch1 and -4 (40, 66, 73, 74), PECAM-1 (33), VE-cadherin (22, 27), TIE-2 (57), membrane type 1 MMP (26, 29, 60, 61, 72), and possibly also Kit-ligand (25). Alternatively, the catalytic activity of ADAM15 may also serve to modulate the function of components of the extracellular matrix or of soluble molecules, including serum proteins.

ADAM15 could conceivably also have a direct or indirect role in cell-cell interactions or cell-matrix interaction. Interestingly, human ADAM15 contains an RGD sequence and has been shown to interact with αvβ3 and α5β1 (48, 80), although this sequence is not conserved in mouse or rat ADAM15 (7, 42). These integrins have been shown to play crucial roles in angiogenesis (15, 20, 35, 69, 79), and therefore it is possible that human ADAM15 has a role in angiogenesis by acting as their ligand. However, given that mouse ADAM15 does not bind to αvβ3 in vitro (18), the role of mouse ADAM15 in angiogenesis is most likely not linked to the function of these two integrins. In vitro studies with mouse ADAM15 have uncovered the integrin α9β1 as a potential receptor (18). However, since mice lacking integrin α9β1 develop a chylothorax after birth and die of respiratrory failure (31), it remains to be determined whether the interaction of ADAM15 with this integrin is responsible for the phenotype observed in the present study.

In addition to potential functions of the ectodomain of ADAM15, the cytoplasmic domain of ADAM15 may be involved in regulating angiogenesis, either as part of "outside-in" signaling triggered by an interaction with another protein or by "inside-out" signaling that would affect the function of the ectodomain. The cytoplasmic domain of ADAM15 has been shown to interact with several cytoplasmic proteins, including Src family protein kinases, the adaptor protein Grb2 (54), as well as two molecules that may affect the intracellular maturation of ADAM15, SH3PX1 (SNX9), and endophilin (30). Since Src family kinases are required for VEGF-mediated angiogenesis (16), ADAM15 could possibly be an effector that is directly or indirectly regulated by these kinases.

Little is currently known about how the expression of

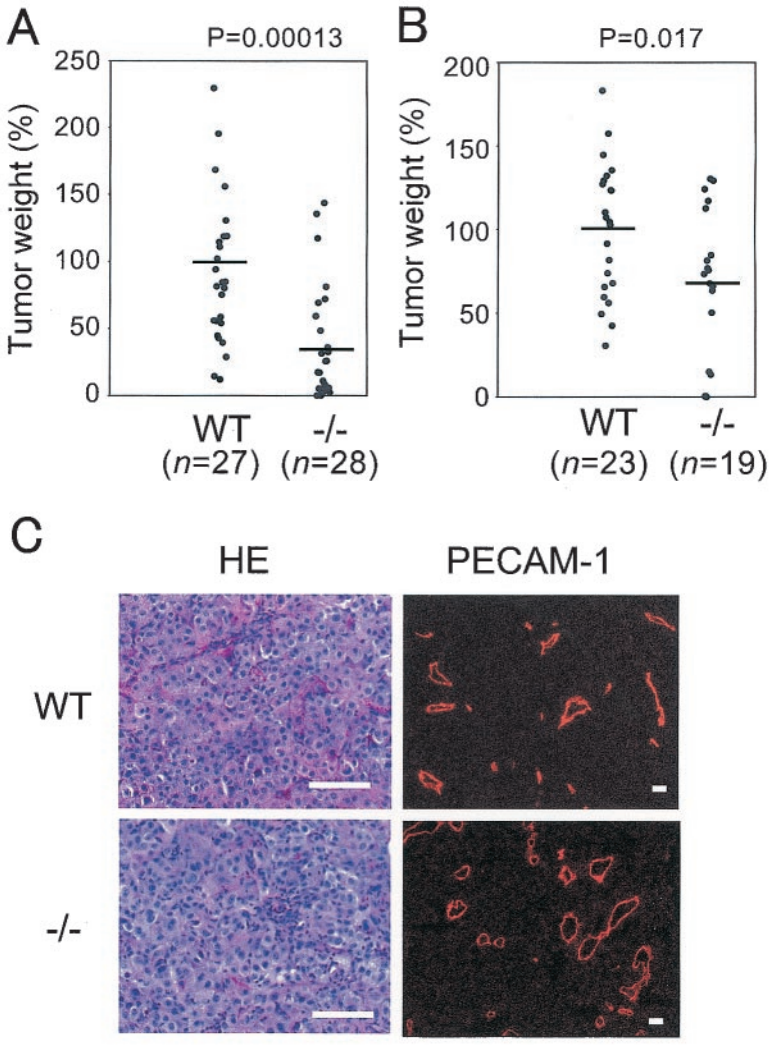

FIG. 7. Tumor growth is retarded in *adam15*$^{-/-}$ mice. Wild-type (WT) and *adam15*$^{-/-}$ (−/−) mice were injected subcutaneously with 10^6 B16F0 cells. (A) Comparison of the final weight of tumors grown in mixed-genetic-background (129/SvJ and C57BL/6) wild-type and *adam15*$^{-/-}$ mice. The results represent the combination of five independent experiments. (B) Comparison of the final weight of the tumors grown in wild-type and *adam15*$^{-/-}$ mice in a predominantly C57BL/6 background (six backcrosses). The data represent the combination of three independent experiments. To account for possible differences in the number of injected cells and their growth potential between individual experiments, as well as different durations of the experiments, the average tumor weight in wild-type animals in each experiment was used as a reference to calculate the weight of each tumor in percentages of this average. The bars in panels A and B represent the average value for wild-type and *adam15*$^{-/-}$ mice. (C) Sections of the tumors grown in wild-type and *adam15*$^{-/-}$ mice stained with hematoxylin and eosin or immunostained with anti-PECAM-1 antibody. No apparent difference in histological morphology or vascular density was observed between the two genotypes. Scale bar, 100 μm.

ADAM15 is regulated (28). The results of the present study show that ADAM15 expression is enhanced in the retinas of mice that are subjected to the ROP model. Since VEGF is essential for retinal neovascularization (36) and is upregulated upon hypoxia (11, 53), we tested whether VEGF might regulate ADAM15 expression in HUVECs. However, the level of ADAM15 protein in HUVECs treated with VEGF was comparable to that in untreated HUVECs. These results are consistent with a gene expression profiling experiment in HUVECs after stimulation with VEGF (1), in which no changes in the expression of ADAM15 were observed over a 24-h time course (M. Abe and Y. Sato, unpublished data). Similarly, bFGF, another potent angiogenic growth factor, did not elicit changes in ADAM15 expression in HUVECs. Based on these findings, ADAM15 expression is not likely to be regulated by VEGF or bFGF in HUVECs. It remains to be determined how ADAM15 levels are regulated in the ROP model.

In summary, a targeted deletion of the widely expressed and catalytically active ADAM15 suggests that this protein is not essential for mouse development or for adult homeostasis. However, ADAM15 is highly expressed in vascular cells and has a critical role in pathological neovascularization in the ROP model and potentially also in a tumor cell implantation model. Further studies will be necessary to define the mechanism underlying the function of ADAM15 in these models. Since ADAM15 has a role in pathological neovascularization but is apparently not required for normal angiogenesis during

development, it may emerge as an attractive target for the design of angiogenesis inhibitors.

ACKNOWLEDGMENTS

This work was supported by National Institutes of Health grant RO1 GM58668 and Memorial Sloan-Kettering Cancer Center Support grant NCI-P30-CA-08748, by the Samuel and May Rudin Foundation, and by the DeWitt Wallace Fund.

We thank Vera Suarez, Willie H. Mark, Jia-Hui Dong, Joanne Ingenito, and Liz Lacy for assistance and advice in generating *adam15*$^{-/-}$ mice; Byung Lee, Eleanor Spumberg, Thadeous Kacmarczyk, Kenya Parks, and Anthony Zayas for assistance in mouse breeding and genotyping; Howard Petrie for the analysis of B- and T-cell ratio in spleen and peripheral lymphocytes; Mayumi Abe and Yasufumi Sato (Tohoku University, Sendai, Japan) for sharing results of a gene expression analysis of VEGF-treated HUVECs; Taha Merghoub and Pier-Paolo Pandolfi for differential blood counts and hematological analysis; and the MSKCC Transgenic Mouse Facility, Molecular Cytology Core Facility, and Research Animal Resources Facility.

REFERENCES

1. **Abe, M., and Y. Sato.** 2001. cDNA microarray analysis of the gene expression profile of VEGF-activated human umbilical vein endothelial cells. Angiogenesis **4:**289–298.
2. **Alfandari, D., H. Cousin, A. Gaultier, K. Smith, J. M. White, T. Darribere, and D. W. DeSimone.** 2001. *Xenopus* ADAM 13 is a metalloprotease required for cranial neural crest-cell migration. Curr. Biol. **11:**918–930.
3. **Asakura, M., M. Kitakaze, S. Takashima, Y. Liao, F. Ishikura, T. Yoshinaka, H. Ohmoto, K. Node, K. Yoshino, H. Ishiguro, H. Asanuma, S. Sanada, Y. Matsumura, H. Takeda, S. Beppu, M. Tada, M. Hori, and S. Higashiyama.** 2002. Cardiac hypertrophy is inhibited by antagonism of ADAM12 processing of HB-EGF: metalloproteinase inhibitors as a new therapy. Nat. Med. **8:**35–40.
4. **Black, R. A., C. T. Rauch, C. J. Kozlosky, J. J. Peschon, J. L. Slack, M. F. Wolfson, B. J. Castner, K. L. Stocking, P. Reddy, S. Srinivasan, N. Nelson, N. Boiani, K. A. Schooley, M. Gerhart, R. Davis, J. N. Fitzner, R. S. Johnson, R. J. Paxton, C. J. March, and D. P. Cerretti.** 1997. A metalloproteinase disintegrin that releases tumour-necrosis factor-α from cells. Nature **385:** 729–733.
5. **Black, R. A., and J. M. White.** 1998. ADAMs: focus on the protease domain. Curr. Opin. Cell Biol. **10:**654–659.
6. **Blobel, C. P.** 1997. Metalloprotease-disintegrins: links to cell adhesion and cleavage of TNF α and Notch. Cell **90:**589–592.
7. **Bosse, F., G. Petzold, R. Greiner-Petter, U. Pippirs, C. Gillen, and H. W. Muller.** 2000. Cellular localization of the disintegrin CRII-7/rMDC15 mRNA in rat PNS and CNS and regulated expression in postnatal development and after nerve injury. Glia **32:**313–327.
8. **Buxbaum, J. D., K. N. Liu, Y. Luo, J. L. Slack, K. L. Stocking, J. J. Peschon, R. S. Johnson, B. J. Castner, D. P. Cerretti, and R. A. Black.** 1998. Evidence that tumor necrosis factor α converting enzyme is involved in regulated α-secretase cleavage of the Alzheimer amyloid protein precursor. J. Biol. Chem. **273:**27765–27767.
9. **Cal, S., J. M. Freije, J. M. Lopez, Y. Takada, and C. Lopez-Otin.** 2000. ADAM 23/MDC3, a human disintegrin that promotes cell adhesion via interaction with the αvβ3 integrin through an RGD-independent mechanism. Mol. Biol. Cell **11:**1457–1469.
10. **Carmeliet, P., and R. K. Jain.** 2000. Angiogenesis in cancer and other diseases. Nature **407:**249–257.
11. **Chavakis, E., B. Riecke, J. Lin, T. Linn, R. G. Bretzel, K. T. Preissner, M. Brownlee, and H. P. Hammes.** 2002. Kinetics of integrin expression in the mouse model of proliferative retinopathy and success of secondary intervention with cyclic RGD peptides. Diabetologia **45:**262–267.
12. **Cho, C., D. O. Bunch, J. E. Faure, E. H. Goulding, E. M. Eddy, P. Primakoff, and D. G. Myles.** 1998. Fertilization defects in sperm from mice lacking fertilin β. Science **281:**1857–1859.
13. **Cho, C., H. Ge, D. Branciforte, P. Primakoff, and D. G. Myles.** 2000. Analysis of mouse fertilin in wild-type and fertilin β$^{-/-}$ sperm: evidence for C-terminal modification, alpha/beta dimerization, and lack of essential role of fertilin α in sperm-egg fusion. Dev. Biol. **222:**289–295.
14. **Condon, T. P., S. Flournoy, G. J. Sawyer, B. F. Baker, T. K. Kishimoto, and C. F. Bennett.** 2001. ADAM17 but not ADAM10 mediates tumor necrosis factor-alpha and L-selectin shedding from leukocyte membranes. Antisense Nucleic Acid Drug Dev. **11:**107–116.
15. **Eliceiri, B. P., and D. A. Cheresh.** 1999. The role of αv integrins during angiogenesis: insights into potential mechanisms of action and clinical development. J. Clin. Investig. **103:**1227–1230.
16. **Eliceiri, B. P., R. Paul, P. L. Schwartzberg, J. D. Hood, J. Leng, and D. A. Cheresh.** 1999. Selective requirement for Src kinases during VEGF-induced angiogenesis and vascular permeability. Mol. Cell **4:**915–924.
17. **Eto, K., C. Huet, T. Tarui, S. Kupriyanov, H. Z. Liu, W. Puzon-McLaughlin, X. P. Zhang, D. Sheppard, E. Engvall, and Y. Takada.** 2002. Functional classification of ADAMs based on a conserved motif for binding to integrin α9β1: implications for sperm-egg binding and other cell interactions. J. Biol. Chem. **277:**17804–17810.
18. **Eto, K., W. Puzon-McLaughlin, D. Sheppard, A. Sehara-Fujisawa, X. P. Zhang, and Y. Takada.** 2000. RGD-independent binding of integrin α9β1 to the ADAM-12 and -15 disintegrin domains mediates cell-cell interaction. J. Biol. Chem. **275:**34922–34930.
19. **Fambrough, D., D. Pan, G. M. Rubin, and C. S. Goodman.** 1996. The cell surface metalloprotease/disintegrin Kuzbanian is required for axonal extension in *Drosophila*. Proc. Natl. Acad. Sci. USA **93:**13233–13238.
20. **Fassler, R., and M. Meyer.** 1995. Consequences of lack of β1 integrin gene expression in mice. Genes Dev. **9:**1896–1908.
21. **Gutwein, P., S. Mechtersheimer, S. Riedle, A. Stoeck, D. Gast, S. Joumaa, H. Zentgraf, M. Fogel, and P. Altevogt.** 2002. ADAM10-mediated cleavage of L1 adhesion molecule at the cell surface and in released membrane vesicles. FASEB J. **3:**292–294.
22. **Ham, C., B. Levkau, E. W. Raines, and B. Herren.** 2002. ADAM15 is an adherens junction molecule whose surface expression can be driven by VE-cadherin. Exp. Cell Res. **279:**239–247.
23. **Hammes, H. P., M. Brownlee, A. Jonczyk, A. Sutter, and K. T. Preissner.** 1996. Subcutaneous injection of a cyclic peptide antagonist of vitronectin receptor-type integrins inhibits retinal neovascularization. Nat. Med. **2:**529–533.
24. **Hartmann, D., B. de Strooper, L. Serneels, K. Craessaerts, A. Herreman, W. Annaert, L. Umans, T. Lubke, A. Lena Illert, K. von Figura, and P. Saftig.** 2002. The disintegrin/metalloprotease ADAM 10 is essential for Notch signalling but not for α-secretase activity in fibroblasts. Hum. Mol. Genet. **11:**2615–2624.
25. **Heissig, B., K. Hattori, S. Dias, M. Friedrich, B. Ferris, N. R. Hackett, R. G. Crystal, P. Besmer, D. Lyden, M. A. Moore, Z. Werb, and S. Rafii.** 2002. Recruitment of stem and progenitor cells from the bone marrow niche requires MMP-9 mediated release of Kit-ligand. Cell **109:**625–637.
26. **Hernandez-Barrantes, S., M. Toth, M. M. Bernardo, M. Yurkova, D. C. Gervasi, Y. Raz, Q. A. Sang, and R. Fridman.** 2000. Binding of active (57 kDa) membrane type 1-matrix metalloproteinase (MT1-MMP) to tissue inhibitor of metalloproteinase (TIMP)-2 regulates MT1-MMP processing and pro-MMP-2 activation. J. Biol. Chem. **275:**12080–12089.
27. **Herren, B., B. Levkau, E. W. Raines, and R. Ross.** 1998. Cleavage of β-catenin and plakoglobin and shedding of VE-cadherin during endothelial apoptosis: evidence for a role for caspases and metalloproteinases. Mol. Biol. Cell **9:**1589–1601.
28. **Herren, B., E. W. Raines, and R. Ross.** 1997. Expression of a disintegrin-like protein in cultured human vascular cells and in vivo. FASEB J. **11:**173–180.
29. **Hiraoka, N., E. Allen, I. J. Apel, M. R. Gyetko, and S. J. Weiss.** 1998. Matrix metalloproteinases regulate neovascularization by acting as pericellular fibrinolysins. Cell **95:**365–377.
30. **Howard, L., K. K. Nelson, R. A. Maciewicz, and C. P. Blobel.** 1999. Interaction of the metalloprotease disintegrins MDC9 and MDC15 with two SH3 domain-containing proteins, endophilin I and SH3PX1. J. Biol. Chem. **274:** 31693–31699.
31. **Huang, X. Z., J. F. Wu, R. Ferrando, J. H. Lee, Y. L. Wang, R. V. Farese, Jr., and D. Sheppard.** 2000. Fatal bilateral chylothorax in mice lacking the integrin α9β1. Mol. Cell. Biol. **20:**5208–5215.
32. **Iba, K., R. Albrechtsen, B. Gilpin, C. Frohlich, F. Loechel, A. Zolkiewska, K. Ishiguro, T. Kojima, W. Liu, J. K. Langford, R. D. Sanderson, C. Brakebusch, R. Fassler, and U. M. Wewer.** 2000. The cysteine-rich domain of human ADAM 12 supports cell adhesion through syndecans and triggers signaling events that lead to β1 integrin-dependent cell spreading. J. Cell Biol. **149:**1143–1156.
33. **Ilan, N., A. Mohsenin, L. Cheung, and J. A. Madri.** 2001. PECAM-1 shedding during apoptosis generates a membrane-anchored truncated molecule with unique signaling characteristics. FASEB J. **15:**362–372.
34. **Kawaguchi, N., X. Xu, R. Tajima, P. Kronqvist, C. Sundberg, F. Loechel, R. Albrechtsen, and U. M. Wewer.** 2002. ADAM 12 protease induces adipogenesis in transgenic mice. Am. J. Pathol. **160:**1895–1903.
35. **Kim, S., K. Bell, S. A. Mousa, and J. A. Varner.** 2000. Regulation of angiogenesis in vivo by ligation of integrin α1β5 with the central cell-binding domain of fibronectin. Am. J. Pathol. **156:**1345–1362.
36. **Klagsbrun, M., and P. A. D'Amore.** 1996. Vascular endothelial growth factor and its receptors. Cytokine Growth Factor Rev. **7:**259–270.
37. **Kratzschmar, J., L. Lum, and C. P. Blobel.** 1996. Metargidin, a membrane-anchored metalloprotease-disintegrin protein with an RGD integrin binding sequence. J. Biol. Chem. **271:**4593–4596.
38. **Kronqvist, P., N. Kawaguchi, R. Albrechtsen, X. Xu, H. D. Schroder, B. Moghadaszadeh, F. C. Nielsen, C. Frohlich, E. Engvall, and U. M. Wewer.** 2002. ADAM12 alleviates the skeletal muscle pathology in mdx dystrophic mice. Am. J. Pathol. **161:**1535–1540.
39. **Kurisaki, T., A. Masuda, K. Sudo, J. Sakagami, S. Higashiyama, Y. Matsuda, A. Nagabukuro, A. Tsuji, Y. Nabeshima, M. Asano, Y. Iwakura, and A. Sehara-Fujisawa.** 2003. Phenotypic analysis of Meltrin α (ADAM12)-defi-

cient mice: involvement of Meltrin α in adipogenesis and myogenesis. Mol. Cell. Biol. **23:**55–61.
40. **Leong, K. G., X. Hu, L. Li, M. Noseda, B. Larrivee, C. Hull, L. Hood, F. Wong, and A. Karsan.** 2002. Activated Notch4 inhibits angiogenesis: role of β1-integrin activation. Mol. Cell. Biol. **22:**2830–2841.
41. **Lieber, T., S. Kidd, and M. W. Young.** 2002. kuzbanian-mediated cleavage of *Drosophila* Notch. Genes Dev. **16:**209–221.
42. **Lum, L., M. S. Reid, and C. P. Blobel.** 1998. Intracellular maturation of the mouse metalloprotease disintegrin MDC15. J. Biol. Chem. **273:**26236–26247.
43. **Manova, K., K. Nocka, P. Besmer, and R. F. Bachvarova.** 1990. Gonadal expression of c-kit encoded at the W locus of the mouse. Development **110:**1057–1069.
44. **Martin, J., L. V. Eynstone, M. Davies, J. D. Williams, and R. Steadman.** 2002. The role of ADAM 15 in glomerular mesangial cell migration. J. Biol. Chem. **277:**33683–33689.
45. **Merlos-Suarez, A., S. Ruiz-Paz, J. Baselga, and J. Arribas.** 2001. Metalloprotease-dependent protransforming growth factor-α ectodomain shedding in the absence of tumor necrosis factor-α-converting enzyme. J. Biol. Chem. **276:**48510–48517.
46. **Mitchell, K. J., K. I. Pinson, O. G. Kelly, J. Brennan, J. Zupicich, P. Scherz, P. A. Leighton, L. V. Goodrich, X. Lu, B. J. Avery, P. Tate, K. Dill, E. Pangilinan, P. Wakenight, M. Tessier-Lavigne, and W. C. Skarnes.** 2001. Functional analysis of secreted and transmembrane proteins critical to mouse development. Nat. Genet. **28:**241–249.
47. **Moss, M. L., S. L. Jin, M. E. Milla, D. M. Bickett, W. Burkhart, H. L. Carter, W. J. Chen, W. C. Clay, J. R. Didsbury, D. Hassler, C. R. Hoffman, T. A. Kost, M. H. Lambert, M. A. Leesnitzer, P. McCauley, G. McGeehan, J. Mitchell, M. Moyer, G. Pahel, W. Rocque, L. K. Overton, F. Schoenen, T. Seaton, J. L. Su, J. D. Becherer, et al.** 1997. Cloning of a disintegrin metalloproteinase that processes precursor tumour-necrosis factor-α. Nature **385:**733–736.
48. **Nath, D., P. M. Slocombe, P. E. Stephens, A. Warn, G. R. Hutchinson, K. M. Yamada, A. J. Docherty, and G. Murphy.** 1999. Interaction of metargidin (ADAM-15) with αvβ3 and α5β1 integrins on different haemopoietic cells. J. Cell Sci. **112:**579–587.
49. **Nath, D., P. M. Slocombe, A. Webster, P. E. Stephens, A. J. Docherty, and G. Murphy.** 2000. Meltrin gamma(ADAM-9) mediates cellular adhesion through $\alpha_6\beta_1$ integrin, leading to a marked induction of fibroblast cell motility. J. Cell Sci. **113:**2319–2328.
50. **Nishimura, H., C. Cho, D. R. Branciforte, D. G. Myles, and P. Primakoff.** 2001. Analysis of loss of adhesive function in sperm lacking cyritestin or fertilin β. Dev. Biol. **233:**204–213.
51. **Pan, D., and G. M. Rubin.** 1997. Kuzbanian controls proteolytic processing of Notch and mediates lateral inhibition during *Drosophila* and vertebrate neurogenesis. Cell **90:**271–280.
52. **Peschon, J. J., J. L. Slack, P. Reddy, K. L. Stocking, S. W. Sunnarborg, D. C. Lee, W. E. Russell, B. J. Castner, R. S. Johnson, J. N. Fitzner, R. W. Boyce, N. Nelson, C. J. Kozlosky, M. F. Wolfson, C. T. Rauch, D. P. Cerretti, R. J. Paxton, C. J. March, and R. A. Black.** 1998. An essential role for ectodomain shedding in mammalian development. Science **282:**1281–1284.
53. **Pierce, E. A., R. L. Avery, E. D. Foley, L. P. Aiello, and L. E. Smith.** 1995. Vascular endothelial growth factor/vascular permeability factor expression in a mouse model of retinal neovascularization. Proc. Natl. Acad. Sci. USA **92:**905–909.
54. **Poghosyan, Z., S. M. Robbins, M. D. Houslay, A. Webster, G. Murphy, and D. R. Edwards.** 2002. Phosphorylation-dependent interactions between ADAM15 cytoplasmic domain and Src family protein-tyrosine kinases. J. Biol. Chem. **277:**4999–5007.
55. **Primakoff, P., and D. G. Myles.** 2000. The ADAM gene family: surface proteins with adhesion and protease activity. Trends Genet. **16:**83–87.
56. **Qi, H., M. D. Rand, X. Wu, N. Sestan, W. Wang, P. Rakic, T. Xu, and S. Artavanis-Tsakonas.** 1999. Processing of the notch ligand delta by the metalloprotease Kuzbanian. Science **283:**91–94.
57. **Reusch, P., B. Barleon, K. Weindel, G. Martiny-Baron, A. Godde, G. Siemeister, and D. Marme.** 2001. Identification of a soluble form of the angiopoietin receptor TIE-2 relased from endothelial cells and present in human blood. Angiogenesis **4:**123–131.
58. **Robertson, E. J.** 1987. Emryo derived stem cell lines, p. 71–112. *In* E. J. Robertson (ed.), Teratocarcinomas and embryonic stem cells: a practical approach. IRL Press, Oxford, United Kingdom.
59. **Rooke, J., D. Pan, T. Xu, and G. M. Rubin.** 1996. KUZ, a conserved metalloprotease-disintegrin protein with two roles in *Drosophila* neurogenesis. Science **273:**1227–1231.
60. **Sato, H., T. Kinoshita, T. Takino, K. Nakayama, and M. Seiki.** 1996. Activation of a recombinant membrane type 1-matrix metalloproteinase (MT1-MMP) by furin and its interaction with tissue inhibitor of metalloproteinases (TIMP)-2. FEBS Lett. **393:**101–104.
61. **Sato, H., T. Takino, Y. Okada, J. Cao, A. Shinagawa, E. Yamamoto, and M. Seiki.** 1994. A matrix metalloproteinase expressed on the surface of invasive tumour cells. Nature **370:**61–65.
62. **Schlondorff, J., and C. P. Blobel.** 1999. Metalloprotease-disintegrins: modular proteins capable of promoting cell-cell interactions and triggering signals by protein-ectodomain shedding. J. Cell Sci. **112:**3603–3617.
63. **Seals, D. F., and S. A. Courtneidge.** 2003. The ADAMs familiy of metalloproteases: multidomain proteins with multiple functions. Genes Dev. **17:**7–30.
64. **Shamsadin, R., I. M. Adham, K. Nayernia, U. A. Heinlein, H. Oberwinkler, and W. Engel.** 1999. Male mice deficient for germ-cell cyritestin are infertile. Biol. Reprod. **61:**1445–1451.
65. **Shirakabe, K., S. Wakatsuki, T. Kurisaki, and A. Fujisawa-Sehara.** 2001. Roles of Meltrin β/ADAM19 in the processing of neuregulin. J. Biol. Chem. **276:**9352–9358.
66. **Shirayoshi, Y., Y. Yuasa, T. Suzuki, K. Sugaya, E. Kawase, T. Ikemura, and N. Nakatsuji.** 1997. Proto-oncogene of int-3, a mouse Notch homologue, is expressed in endothelial cells during early embryogenesis. Genes Cells **2:**213–224.
67. **Smith, L. E., E. Wesolowski, A. McLellan, S. K. Kostyk, R. D'Amato, R. Sullivan, and P. A. D'Amore.** 1994. Oxygen-induced retinopathy in the mouse. Investig. Ophthalmol. Vis. Sci. **35:**101–111.
68. **Sotillos, S., F. Roch, and S. Campuzano.** 1997. The metalloprotease-disintegrin Kuzbanian participates in Notch activation during growth and patterning of *Drosophila* imaginal discs. Development **124:**4769–4779.
69. **Stephens, L. E., A. E. Sutherland, I. V. Klimanskaya, A. Andrieux, J. Meneses, R. A. Pedersen, and C. H. Damsky.** 1995. Deletion of β1 integrins in mice results in inner cell mass failure and peri-implantation lethality. Genes Dev. **9:**1883–1895.
70. **Sunnarborg, S. W., C. L. Hinkle, M. Stevenson, W. E. Russell, C. S. Raska, J. J. Peschon, B. J. Castner, M. J. Gerhart, R. J. Paxton, R. A. Black, and D. C. Lee.** 2002. Tumor necrosis factor-α converting enzyme (TACE) regulates epidermal growth factor receptor ligand availability. J. Biol. Chem. **277:**12838–12845.
71. **Thodeti, C. K., R. Albrechtsen, M. Grauslund, M. Asmar, C. Larsson, Y. Takada, A. M. Mercurio, J. R. Couchman, and U. M. Wewer.** 2002. ADAM12/syndecan-4 signaling promotes β 1 integrin-dependent cell spreading through PKCα and RhoA. J. Biol. Chem. **31:**9576–9584.
72. **Toth, M., S. Hernandez-Barrantes, P. Osenkowski, M. M. Bernardo, D. C. Gervasi, Y. Shimura, O. Meroueh, L. P. Kotra, B. G. Galvez, A. G. Arroyo, S. Mobashery, and R. Fridman.** 2002. Complex pattern of membrane type 1 matrix metalloproteinase shedding: regulation by autocatalytic cells surface inactivation of active enzyme. J. Biol. Chem. **277:**26340–26350.
73. **Uyttendaele, H., J. Ho, J. Rossant, and J. Kitajewski.** 2001. Vascular patterning defects associated with expression of activated Notch4 in embryonic endothelium. Proc. Natl. Acad. Sci. USA **98:**5643–5648.
74. **Uyttendaele, H., G. Marazzi, G. Wu, Q. Yan, D. Sassoon, and J. Kitajewski.** 1996. Notch4/int-3, a mammary proto-oncogene, is an endothelial cell-specific mammalian Notch gene. Development **122:**2251–2259.
75. **Wen, C., M. M. Metzstein, and I. Greenwald.** 1997. SUP-17, a *Caenorhabditis elegans* ADAM protein related to *Drosophila* KUZBANIAN, and its role in LIN-12/NOTCH signalling. Development **124:**4759–4767.
76. **Weskamp, G., H. Cai, T. A. Brodie, S. Higashyama, K. Manova, T. Ludwig, and C. P. Blobel.** 2002. Mice lacking the metalloprotease-disintegrin MDC9 (ADAM9) have no evident major abnormalities during development or adult life. Mol. Cell. Biol. **22:**1537–1544.
77. **Weskamp, G., J. Kratzschmar, M. S. Reid, and C. P. Blobel.** 1996. MDC9, a widely expressed cellular disintegrin containing cytoplasmic SH3 ligand domains. J. Cell Biol. **132:**717–726.
78. **Yagi, T., Y. Ikawa, K. Yoshida, Y. Shigetani, N. Takeda, I. Mabuchi, T. Yamamoto, and S. Aizawa.** 1990. Homologous recombination at c-fyn locus of mouse embryonic stem cells with use of diphtheria toxin A-fragment gene in negative selection. Proc. Natl. Acad. Sci. USA **87:**9918–9922.
79. **Yang, J. T., H. Rayburn, and R. O. Hynes.** 1993. Embryonic mesodermal defects in α_5 integrin-deficient mice. Development **119:**1093–1105.
80. **Zhang, X. P., T. Kamata, K. Yokoyama, W. Puzon-McLaughlin, and Y. Takada.** 1998. Specific interaction of the recombinant disintegrin-like domain of MDC-15 (metargidin, ADAM-15) with integrin $\alpha_v\beta_3$. J. Biol. Chem. **273:**7345–7350.